Published in final edited form as:
Chemphyschem. 2008 August 25; 9(12): 1673–1679. doi:10.1002/cphc.200800296.

Oxygen Microscopy by Two-Photon-Excited Phosphorescence

Olga S. Finikova[a], **Artem Y. Lebedev**[a], **Alexey Aprelev**[b], **Thomas Troxler**[c], **Feng Gao**[c], **Carmen Garnacho**[d], **Silvia Muro**[d], **Robin M. Hochstrasser**[c], and **Sergei A. Vinogradov**[a,*]

a *Department of Biochemistry and Biophysics, University of Pennsylvania, Philadelphia PA 19104-6059 (USA), Fax: (+1) 215-573-3787*

b *Department of Physics, Drexel University, Philadelphia, PA 19104 (USA)*

c *Department of Chemistry and RLBL, University of Pennsylvania, Philadelphia, PA 19104 (USA)*

d *Department of Pharmacology, University of Pennsylvania, Philadelphia, PA 19104 (USA)*

Abstract

High-resolution images of oxygen distributions in microheterogeneous samples are obtained by two-photon laser scanning microscopy (2P LSM), using a newly developed dendritic nanoprobe with internally enhanced two-photon absorption (2PA) cross-section. In this probe, energy is harvested by a 2PA antenna, which passes excitation onto a phosphorescent metalloporphyrin via intramolecular energy transfer. The 2P LSM allows sectioning of oxygen gradients with near diffraction-limited resolution, and lifetime-based acquisition eliminates dependence on the local probe concentration. The technique is validated on objects with a priori known oxygen distributions and applied to imaging of pO_2 in cells.

Keywords

dendrimer; energy transfer; oxygen; phosphorescence; porphyrin

1. Introduction

Imaging of oxygen distributions is of key importance for several areas of physiology and medicine. For example, in neuroscience, the ability to image brain oxygenation is critical for understanding neuronal activation;[1] in ophthalmology, imaging of retinal pO_2 (partial oxygen pressure) can help elucidating causes of diabetic retinopathy and macular degeneration;[2] in photodynamic therapy of cancer, measuring tumor pO_2 will facilitate optimization of treatment protocols, complementing direct imaging of singlet oxygen.[3] Oxygen levels can vary between individual tissue compartments (intravascular vs interstitial vs intracellular), and the ability to quantify changes in partial oxygen pressure (pO_2) between and within these compartments at the microscopic level would provide invaluable information for physiological research.

pO_2 in biological systems can be measured optically by the phosphorescence quenching method,[4,5] using probes with controllable quenching parameters and defined bio-distributions. Such probes are delivered directly into the medium of interest, where they serve as molecular sensors for oxygen. Phosphorescence quenching has been widely used to image oxygen in biological objects, including examples of microscopy.[6–9] Wide area illumination

E-mail: vinograd@mail.med.upenn.edu.

Supporting information for this article is available on the WWW under http://dx.doi.org/10.1002/cphc.200800296.

and CCD-based detection are most commonly used in phosphorescence imaging, as they permit fast acquisition, although at the expense of spatial resolution and 3D capability. Confocal laser scanning microscopy has also been applied as an alternative method to image pO_2. However, either large pinholes (diameter ≈1 mm) were required to compensate for low rates of phosphorescence emission,[10] resulting in low spatial resolution; or probes with short triplet lifetimes and, therefore, low oxygen sensitivity, had to be employed.[11]

Herein we report a new approach to oxygen imaging, which combines principles of the phosphorescence quenching method with two-photon laser scanning microscopy (2P LSM).[12] 2P excitation offers several advantages over linear methods, such as improved depth resolution for 3D imaging and reduced risk of photodamage.[13] In principle, combining 2P LSM and phosphorescence quenching should be a straightforward task;[14] however, phosphorescent probes, typically based on Pt and Pd porphyrins, posses extremely low two-photon absorption (2PA) cross-sections (σ_2).[15] Using these probes, either exceedingly high excitation powers would be required to generate adequate signals, or thousands of phosphorescence decays would have to be averaged in each image pixel, resulting in unacceptably long acquisition periods.

In order to circumvent this problem, an approach to enhance triplet generation via 2P excitation in metalloporphyrins has been proposed,[15,16] whereby excitation energy is captured by several 2P-antenna chromophores and transmitted to metalloporphyrin-core by Förster-type resonance energy transfer (FRET). Recent studies have shown that distances between the antenna and the core, as well as their redox potentials, must be carefully tuned in order to prevent intramolecular quenching of phosphorescence via electron transfer (ET).[17,18]

Herein, we introduce the first practical 2P phosphorescent nanoprobe and demonstrate its application in oxygen imaging. The new technique is validated on microheterogeneously oxygenated phantoms with a priori known oxygen distributions and used to obtain pO_2 images inside endothelial cells.

2. Results and Discussion

2.1. 2P-Enhanced Phosphorescent Probe

Phosphorescent probe PtP-C343—whose structure is shown in Figure 1, and its key properties are summarized in Figure 2—integrates in a single molecular construct all the characteristics required for biological oxygen imaging. The probe was constructed mainly with intravascular and interstitial applications in mind, assuming that the delivery into these tissue compartments can be accomplished by injection. Nevertheless, provided suitable delivery pathways, PtP-C343 can be used in any biological environment, for example to measure intracellular oxygen (vide infra). The size of the probe (~5 nm in folded state) is similar to that of other phosphorescent agents used in the past for tissue oxygen measurements and imaging.[19,20]

Several coumarin-343 (C343) moieties in the molecule of PtP-C343 act as the 2PA antenna, channeling the excitation energy to the Pt porphyrin (PtP) core. The high fluorescence quantum yield of C343 ($\phi_{fl} \approx 0.8–1.0$), combined with the strong absorption of PtP in the Q-band region (λ_{max} = 515 nm, ε = 26,000 M^{-1} cm^{-1}) and large spectral overlap (Figure 2 a) enable efficient fluorescence resonance energy transfer (FRET). Molecular modeling reveals that even in the fully unfolded state, C343-units are separated from the PtP-core by distances shorter than the Förster radius (r_0 = 46 Å). Nevertheless, the experimental FRET efficiency does not exceed 75 %, which is likely due to the partial quenching of the C343 singlet state by intramolecular electron transfer[17] (for detailed photophysical characterization see the Supporting Information).

The choice of C343 (σ_2 = 28 GM at 840 nm; 1 GM= 10^{-50} $cm^4 sphoton^{-1}$) as the 2P antenna was based on the overall efficiency of the phosphorescence, 2PA and FRET. Several 2PA dyes capable of FRET onto Pt porphyrins have been considered, including dyes specifically designed for 2P applications. However, all these dyes induce strong reductive quenching of the porphyrin triplet states by electron transfer,[18] reducing the phosphorescence quantum yield and decreasing the probe's performance. C343 was found to be the least effective quencher. In addition, Pt porphyrin was modified with four electron-donor alkoxy groups, making it a less potent oxidant in the triplet state.

To decrease the rate of electron transfer further, C343 fragments in PtP-C343 were placed at the maximal distance from the PtP core, that is, attached to the termini of the dendritic branches. The folded dendrimer was anticipated to provide an insulating layer between the chromophores.[21] As a result of such redox and distance tuning, the phosphorescence quantum yield of Pt-C343 (ϕ_p = 0.10) is only slightly below that of the PtP-dendrimer without C343-antenna (ϕ_p = 0.13). Upon 2P excitation (λ_{ex} = 840 nm, 110 fs, 76 MHz repetition rate, average power 0.5 mW), the C343-antenna in PtP-C343 enhances phosphorescence intensity nearly 25-fold compared to the reference Pt porphyrin (Figure 2 b, inset).

The porphyrin core in PtP-C343 is surrounded by poly(arylglycine) (AG) dendrimer.[22] The main functions of the dendrimer are to increase the solubility, prevent aggregation and attenuate the rate of oxygen diffusion in the porphyrin vicinity.[23,24] This rate is represented by the value of quenching constant k_q in the Stern–Volmer relationship, shown in Equation (1), which is the basis for oxygen sensing by phosphorescence quenching:

$$\tau_0/\tau = 1 + k_q \times \tau_0 \times pO_2 \quad (1)$$

In Equation (1), τ and τ_0 are the phosphorescence lifetimes in the absence of oxygen and at oxygen pressure pO_2. Constants k_q for unprotected metalloporphyrins in aqueous solutions are too high (>1500 $mmHg^{-1}$ s^{-1})[24,25] for measurements at physiologically relevant pO_2's (100–160 mm Hg). Hydrophobic dendrimers, such as AG, are capable of attenuating the quenching constants by folding and restricting oxygen diffusion in the porphyrin vicinity.[25]

The periphery of the dendrimer is modified with mono-methyloligoethyleneglycol groups (av. MW 750), which prevent interactions of the probe with proteins and other biological solutes. This is required for maintaining an unambiguous relationship between the phosphorescence lifetime and pO_2, making sure that the probe's signal is specific to oxygen.[25] For example, quenching plots of PtP-C343 remain unchanged in the cell growth medium containing albumin (Figure 2 c), which is known to dramatically affect quenching constants of unprotected porphyrins.[4,25] The same quenching constants are obtained at different pH values and different probe concentrations. (For calibrations at different temperatures see Supporting Information). Notably, all calibrations under linear (1P) excitation are directly applicable to the measurements in the two-photon regime,[15] since phosphorescence emission and oxygen quenching are independent of the pathway by which the probe is promoted to its emitting state.

A convenient feature of PtP-C343 is the residual fluorescence of C343-antenna. C343 fluorescence is well spectrally resolved from PtP phosphorescence (Figures 2 a, b) and is completely insensitive to oxygen because of its short lifetime (τ_{fl} = 0.21 ns). This signal enables measurements of phosphorescence lifetimes by dual-wavelength ratiometric method.[26,27] Emission spectra of PtP-C343 upon two-photon excitation (λ_{ex} = 840 nm) at different oxygen concentrations (Figure 2c, inset), show that only phosphorescence responds to changes in pO_2.

2.2. Imaging Method

For phosphorescence lifetime measurements in the time domain, excitation pulses must be separated by at least 5–6 lifetimes, that is, 300–400 μs for probes like PtP-C343 (τ_0 =60 μs). Commercial Ti:Sapphire lasers, typically used in 2P LSM, operate at high repetition rates (~100 MHz); therefore, for measuring phosphorescence lifetimes their output must be gated. To determine the optimal excitation regime, we have modeled the kinetics of phosphorescence under 2P excitation which is shown schematically in Figure 3 (see Supporting Information for details). In the scheme, A and P are the 2P-antenna and the phosphorescent core of the probe; indexes S_0, S_1 and T_1 designate the ground, the first excited singlet and triplet states; α, k_{FRET}, k_{fl}, and k_p are the rate constants of absorption (via 2P mechanism), FRET, decay of the S_1 state in the absence of FRET and decay of the T_1 state, respectively.

Using the scheme in Figure 3 and the experimentally measured rate constants ($k_{fl} = 2.5 \times 10^8\ s^{-1}$, $k_p = 1.67 \times 10^4\ s^{-1}$, $k_{FRET} = 2.3 \times 10^9\ s^{-1}$, $\sigma_2 \approx 100$ GM at 840 nm), we have calculated the dependencies of the triplet state fraction (P^{T1}) on the number of high repetition rate laser pulses (Figure 3 a, see Supporting Information for details). For example, at the average power of 10 mW, a gate containing 200 pulses, delivered during 2.5 μs period, fully saturates the phosphorescence of PtP-C343 in the laser focal volume (~2–3 μm^3), yielding 99 % of the probe in its triplet state.

To achieve the maximal (diffraction-limited) resolution, concentration of the emitting species in the vicinity of the focal volume must change in proportion to the square of the excitation flux.[13] Figure 3 b shows the dependence of the triplet state fraction (P^{T1}) on the average laser power for the case when the excitation is delivered by a continuous train of high repetition rate pulses. Deviation from the quadratic dependence becomes apparent when the fraction of the emitting species exceeds 15–20% (Figure 3b). For a long-lived triplet state (τ_0 = 60 μs), which cannot fully decay between the excitation pulses, this limit is reached already at quite low powers (<1 mW), or, if the power is sufficiently high, after a small number of pulses (Figure 3 a). For example, at the average power of 10 mW, 20% saturation requires only about 30–40 pulses (0.4–0.5 μs excitation gate at 76 MHz repetition rate). Notably, beyond the saturation onset, the mechanism of excitation does not change, but the excitation volume increases, resulting in lower spatial resolution.

At the probe concentration of 10^{-5}M and the phosphorescence quantum yield $\phi_p = 0.10$, one excitation gate leading to 20% saturation will generate ca. 300 phosphorescent photons, of which only about 10 % reach the detector. Considering shot-noise-limit detection and the detector quantum yield of ca. 0.10, about 200 gates will be required to achieve the signal-to-noise ratio of 25, suitable for accurate phosphorescence lifetime determination. The setup used in our experiments was not specifically optimized for 2P imaging, and in order to obtain adequate quality decays we had to use at least 1 μs long excitation gates and average laser powers up to 100 mW. Under these conditions, ca. 30 photons were obtained per excitation gate per pixel. Presumably, the excitation volume in our experiments was larger than the diffraction-limit.

Unlike phosphorescence, fluorescence of C343 antenna has ample time to decay between the high repetition rate pulses. As a result, the onset of the fluorescence saturation occurs at much higher average laser powers. This has implications for imaging in dual-wavelength ratiometric mode, in which the ratio of the fluorescence and phosphorescence signals is used to measure phosphorescence lifetime τ.[26] In order for calibrations to be independent of the excitation regime, power dependencies of both signals must be the same, that is, the signals have to change in proportion to one another with changes in the excitation power. Consequently, 2P ratiometric measurements are feasible only at very low powers, where both the fluorescence and the

phosphorescence signals are strictly proportional to the square of the excitation flux (Figure 3 b).

2.3. Imaging Heterogeneously Oxygenated Objects

Testing the method's ability to resolve microscopic oxygen gradients requires an object with a priori known oxygen distribution. An ultra-thin glass capillary, filled with a solution of PtP-C343 (10 μM) and containing an excess of enzymatic system for oxygen removal (glucose/glucose oxidase/catalase),[4] was fixed at an angle relative to a microscope coverslip (Figure 4), and its tip (0.5 μm in diameter) was covered with the probe solution equilibrated with air. The mixing between the outside and inside medium was slow; and in addition, a large excess of the oxygen-depleting system guaranteed rapid removal of oxygen inside the capillary, while the solution outside could freely exchange oxygen with air.

The first indication that the 2P-excited phosphorescence signal contained information about oxygen in the object was obtained from the integrated intensity image under pseudo-continuous excitation by a non-gated train of pulses (Figure 4 b). The capillary appears as a bright stripe (capillary walls are bright because of the back-scattering on the glass/water interface), and the phosphorescence/fluorescence ratios in the spectra from the areas inside and outside the capillary (Figure 4 c) correspond to the calibrations (Figure 2 c).

The phosphorescence lifetime images were obtained by gating the output of a high repetition rate Ti:Sapphire laser (840 nm, 110 fs, 76 MHz, 1 μs excitation gate). Figure 4 e clearly shows the region of lower oxygenation (τ = 40–50 μs) relative to the normally aerated background (τ = 32 μs). The contrast decreases towards the open capillary tip (Figure 4 f), where mixing with the outside solution is more effective. In a stacked 3D-image, obtained by *x*,*y*-raster-scanning at 5 μm steps in the *z*-direction, the capillary appears as a tube with the cross-section elongated in the *z*-direction. This distortion is caused by the excitation volume asymmetry [28] and by the refraction on the glass/water interface. Nevertheless, this experiment clearly demonstrates the ability of the method to provide pO_2 images throughout the volume depth.

Single-exponential fitting of the decays obtained by averaging of 100 gates results in the accuracy of ±0.6 μs in lifetime τ, which is equivalent to ±2.5 mm Hg accuracy in pO_2 (in the low oxygen region). Higher accuracy can be reached by increasing the range of measured lifetimes τ, for example, by increasing constant k_q [Eq. (1)].

For a given lifetime τ_0, which is intrinsic to the phosphorescent chromophore, the range of measured lifetimes through the range of oxygen concentrations (from 0 to 159 mm Hg in biological systems) is determined by the value of quenching constant k_q [Eq. (1)]; which is, in turn, dependent on the chromophore accessibility to oxygen. For chromophores with short τ_0's, too low k_q's lead to narrow dynamic ranges. Taking into account relatively short τ_0 of Pt porphyrin (60 μs), the dendritic branches in PtP-C343 were attached to the *para*-positions of the *meso*-aryl rings (Figure 1) in order to keep the core more accessible to oxygen. (A much stronger protection would be expected for 3,5-*meta*-orientation[25,29]). Nonetheless, k_q appeared to be lower than expected, that is, ~150 mm $Hg^{-1}s^{-1}$ vs expected 400–500 mm $Hg^{-1}s^{-1}$, resulting in the dynamic lifetime range of 40 μs. Using smaller, more oxygen-permeable shells, for example, polyglutamic[24] or Newkome-type dendrimers,[30] will allow extending the range of τ's. Alternatively, Pd porphyrins, whose intrinsic phosphorescence lifetimes are much longer (300–700 μs)[4,24] can be used; however, these chromophores have lower phosphorescence quantum yields and therefore necessitate longer acquisition periods.

2.4. Imaging Oxygen in Cells

Mapping of intracellular pO_2 provides direct insight into the environment of cellular organelles and compartments, simultaneously helping to define the range of the method's applicability. Ideally, measurements of intracellular pO_2 require the probe to be distributed throughout the cytoplasm volume.[7] However, delivering macromolecular constructs into the cytoplasm without affecting the cell viability is a challenging and yet unachieved goal.[31] It is more feasible to incorporate the probe into the cell by endocytic transport within vesicles,[31,32] whose interiors are separated from the cytoplasm by oxygen-permeable membranes.

We used a method for endocytic delivery[33] into human endothelial cells (ECs), which employs intercellular adhesion molecule-1 (ICAM-1).[34] Engagement of ICAM-1 by multivalent ligands on surfaces of microscopic objects, in our case latex microspheres coated with anti-ICAM, triggers formation of endocytic compartments. The probes present in the extracellular milieu become a part of the liquid phase surrounding the microspheres within the endocytic vesicles. The latter pinch off the plasma membrane into the cytosol and traffic intracellularly to the perinuclear region,[32,33] where the probe can function as a pO_2-sensor. In addition, microspheres create easily recognizable heterogeneous patterns around the nuclei, facilitating visualization.

Linear fluorescent microscopy (Figure 5 a, b) confirmed that PtP-C343 was co-internalized by ECs from the cell medium together with anti-ICAM-modified microspheres. Neither the cell viability nor the efficiency of uptake was affected by the presence of the probe (used at 10 μM oncentration). The internalized microspheres form characteristic perinuclear clusters, whereas the non-internalized microspheres remain on the cell periphery and do not co-localize with the probe (for control experiments see Supporting Information). A fraction of the probe was passively internalized within 100–200 nm endocytic vesicles without spheres, which also trafficked to the perinuclear region.

Integrated intensity image of phosphorescence (Figure 5 d), acquired upon 2PA-excitation, reveals that the emission was predominantly co-localized with the signal observed in the red-channel of a regular fluorescent microscope (Figure 5 b). All six microspheres in the image (Figure 5 c, inside the white square) were among the brightest emitters, and some appeared as characteristic ring-like objects. These patterns occur when the scanning plane dissects *endo*-lysosomes, containing non-emissive microspheres surrounded by the probe solution. Phosphorescence decay times (Figure 5 e) are uniformly distributed around τ_{av} = 33.1 μs, agreeing well with the calibration measurement (τ=33.9 ± 3 μs). Only the emission from the perinuclear region (area 3, Figure 5 g) contains a characteristic phosphorescence peak in the spectrum (λ_{max} = 680 nm).

The phosphorescence lifetime and the pO_2 images of live cells (Figures 5 h, i) revealed that the average oxygen pressures in the vicinity of the nuclei [for image shown: pO_2(mean) = 156.9 mm Hg] are close to the pO_2 in air-equilibrated aqueous medium. The value of the intracellular pO_2 gradient, although determined by indirect measurements nearly two decades ago,[35] is still a controversial subject in the literature. Intracellular 2P oxygen imaging in vivo is able to definitively establish its value.

3. Conclusions

We have introduced a two-photon enhanced phosphorescent nanoprobe that makes it possible to combine the 2P LSM with the phosphorescence quenching method. Compared with existing pO_2 measurement techniques,[36–39] this approach possesses an unprecedented combination of high spatial and temporal resolution, minimal invasiveness and 3D capability. The 2P oxygen microscopy is expected to have its largest impact in the studies of intact tissues in vivo,

where accurate non-invasive determination of oxygen concentration is the key to understanding physiological function.

Experimental Section

Probe design—Probe PtP-C343 was synthesized using mixed divergent/convergent approach. Four butyl-ester-terminated generation 3 arylglycine (AG) dendrons were coupled to the core Pt porphyrin, after which the peripheral ester groups were hydrolyzed. C343-fragments, modified with ethylenediamine linkers, were attached to the dendrimer periphery, and the remaining carboxyl groups were esterified with oligoethyleneglycol residues (Av. MW 750). The probe was purified by size exclusion chromatography and multiple re-precipitations from THF by ether. The intermediate compounds and the product were characterized by ^{1}H, ^{13}C NMR and MALDI-TOF spectroscopy. Details of the photophysical and electrochemical characterization, calculations, measurements of FRET rates and two-photon absorption cross-sections can found in the Supporting Information.

Imaging system—Imaging experiments were performed using the system shown in Figure 6. The 2P-excitation was achieved by a mode-locked Ti:sapphire oscillator (λ_{ex} = 840 nm, 110 fs, 76 MHz rep. rate, Mira 900, Coherent). An electro-optical modulator (Con-Optics) played the role of the beam chopper. The beam was directed into the oil immersion objective (170 μm focal distance, NA 1.3, Nikon) of an inverted confocal microscope (Nikon Diaphot 300), equipped with a scanning stage (Queensgate, scanning area 30×30 μm^2). The emission signal, after passing through a series of filters, was directed onto one or two single-photon counting APDs (EG&G). Alternatively, the emission beam was directed through a monochromator (Acton Research) to a cooled CCD camera (Princeton Instruments) for spectral registration. For ratiometric imaging, the emission beam was passed through a dichroic beam splitter (565DCXR, Chroma) in order to separate fluorescence of C343 (λ_{max} = 485 nm) from phosphorescence of PtP (λ_{max} = 670 nm). For time-gated operation, the software for control of the scanning stage and the photon counting was custom-designed in LabView 7.0 (National Instruments). In a typical run, the frequency of the electro-optical modulator was set to 2 kHz. The pulse-train length of the excitation gate was adjusted between 1 and 2 μs, allowing for several hundreds laser pulses to pass through the modulator. The collection period between consecutive excitation gates (0.5 ms) was divided into 50 bins. 5 to 200 averages were used to collect decays, depending on the experiment.

Preparation of Cells—Mouse monoclonal antibody recognizing the extracellular domain of human ICAM-1 (clone R6.5) was purified by affinity chromatography from the corresponding hybridoma cell line (American Type Culture Collection, Manassas, VA). Anti-ICAM microspheres were prepared by surface absorption of anti-ICAM R6.5 onto either FITC-labeled or non-fluorescent polystyrene microspheres (2 μm diameter, Polysciences Inc., Warrington, PA) at 7,000 IgG molecules per μm^2 of particle surface. Lack of aggregation and final diameter of the coated particles was determined by dynamic light scattering. Human umbilical vein Endothelial cells, EC (Clonetics, San Diego, CA), were seeded onto gelatin-coated cover slips in plastic well plates, grown in supplemented M199 medium (GibcoBRL, Grand Island, NY) and treated overnight with 10 $ngmL^{-1}$ TNF-α to stimulate ICAM-1 expression. To induce endocytosis in EC, confluent activated cells were first incubated for 30 min at 37°C with FITC-labeled anti-ICAM microspheres, either in the absence or presence of PtP-C343 (10 μM) in the cell media. To permit further intracellular trafficking of the internalized materials, cells were washed and incubated for 30–120 additional min at 37°C. To induce incorporation of PtP-C343 within EC endosomes, EC were incubated with non-fluorescent anti-ICAM microspheres in the presence of PtP-C343. When required, the cell nuclei were stained with blue 4′,6-diamidino-2-phenylindole (DAPI) for 5 min at room temperature, and cells were imaged either prior or after fixation in cold 2% paraformaldehyde.

Acknowledgements

Support of the grants EB007279, HL081273 and P41-RR001348 from the NIH USA is gratefully acknowledged. The authors thank Prof. D. F. Wilson for many invaluable discussions.

References

1. Thompson JK, Peterson MR, Freeman RD. Science 2003;299:1070. [PubMed: 12586942]
2. Arden GB, Sidman RL, Arap W, Schlingemann RO. Br J Ophthalmol 2005;89:764. [PubMed: 15923516]
3. Skovsen E, Snyder JW, Ogilby PR. Photochem Photobiol 2006;82:1187. [PubMed: 16706601]
4. Vanderkooi JM, Maniara G, Green TJ, Wilson DF. J Biol Chem 1987;262:5476. [PubMed: 3571219]
5. Rumsey WL, Vanderkooi JM, Wilson DF. Science 1988;241:1649. [PubMed: 3420417]
6. Shonat RD, Kight AC. Ann Biomed Eng 2003;31:1084. [PubMed: 14582611]
7. Hogan MC. J Appl Physiol 1999;86:720. [PubMed: 9931213]
8. Wilson DF, Vinogradov SA, Grosul P, Vaccarezza MN, Kuroki A, Bennett J. Appl Opt 2005;44:5239. [PubMed: 16149347]
9. Golub AS, Barker MC, Pittman RN. Am J Physiol Heart Circ Physiol 2007;293:H1097. [PubMed: 17483242]
10. Plant RL, Burns DH. Appl Spectrosc 1993;47:1594.
11. Koo YEL, Cao YF, Kopelman R, Koo SM, Brasuel M, Philbert MA. Anal Chem 2004;76:2498. [PubMed: 15117189]
12. Denk W, Strickler JH, Webb WW. Science 1990;248:73. [PubMed: 2321027]
13. Denk, W.; Piston, DW.; Webb, WW. Handbook of Biological Confocal Microscopy. Pawley, JB., editor. Springer; New York: 2006. p. 535-549.
14. Excitation of a Pd porphyrin by 10 ns pulses at 1064 nm (10 Hz repetition rate) has been reported to produce detectable phosphorescence signals at high excitation powers (0.1–1.0 W) and high probe concentration (0.5 mM): Mik EG, van Leeuwen TG, Raat NJ, Ince C. J Appl Physiol 2004;97:1962. [PubMed: 15247164]
15. Briñas RP, Troxler T, Hochstrasser RM, Vinogradov SA. J Am Chem Soc 2005;127:11 851.
16. Dichtel WR, Serin JM, Edder C, Fréchet JMJ, Matuszewski M, Tan LS, Ohulchanskyy TY, Prasad PN. J Am Chem Soc 2004;126:5380. [PubMed: 15113208]
17. Finikova OS, Troxler T, Senes A, DeGrado WF, Hochstrasser RM, Vinogradov SA. J Phys Chem A 2007;111:6977. [PubMed: 17608457]
18. Finikova OS, Chen P, Ou Z, Kadish KM, Vinogradov SA. J Photo-chem Photobiol A 2008;198:75.
19. Rietveld IB, Kim E, Vinogradov SA. Tetrahedron 2003;59:3821.
20. Wilson DF, Lee WMF, Makonnen S, Finikova O, Apreleva S, Vinogradov SA. J Appl Physiol 2006;101:1648. [PubMed: 16888050]
21. Hong YR, Gorman CB. Langmuir 2006;22:10506. [PubMed: 17129022]
22. Vinogradov SA. Org Lett 2005;7:1761. [PubMed: 15844900]
23. Issberner J, Vögtle F, De Cola L, Balzani V. Chem Eur J 1997;3:706.
24. Vinogradov SA, Lo LW, Wilson DF. Chem Eur J 1999;5:1338.
25. Rozhkov VV, Wilson DF, Vinogradov SA. Macromolecules 2002;35:1991.
26. Kostov Y, Harms P, Pilato RS, Rao G. Analyst 2000;125:1175. [PubMed: 10932860]
27. Xu H, Aylott JW, Kopelman R, Miller TJ, Philbert MA. Anal Chem 2001;73:4124. [PubMed: 11569801]
28. Sun HB, Tanaka T, Kawata S. Appl Phys Lett 2002;80:3673.
29. Tomoyose Y, Jiang DL, Jin RH, Aida T, Yamashita T, Horie K, Yashima E, Okamoto Y. Macromolecules 1996;29:5236.
30. Newkome GR, Lin XF. Macromolecules 1991;24:1443.
31. Medina-Kauwe LK, Xie J, Hamm-Alvarez S. Gene Ther 2005;12:1734. [PubMed: 16079885]
32. Muro S, Gajewski C, Koval M, Muzykantov VR. Blood 2005;105:650. [PubMed: 15367437]

33. Muro S, Wiewrodt R, Thomas A, Koniaris L, Albelda SM, Muzykantov VR, Koval M. J Cell Sci 2003;116:1599. [PubMed: 12640043]

34. Dustin ML, Rothlein R, Bhan AK, Dinarello CA, Springer TA. J Immunol 1986;137:245. [PubMed: 3086451]

35. Robiolio M, Rumsey WL, Wilson DF. Am J Physiol 1989;256:C1207. [PubMed: 2735396]

36. Jobsis FF. Science 1977;198:1264. [PubMed: 929199]

37. Koch CJ. Redox Cell Biology and Genetics, Part A. Methods Enzymol 2002;352:3. [PubMed: 12125356]

38. Swartz HM, Clarkson RB. Phys Med Biol 1998;43:1957. [PubMed: 9703059]

39. Krishna MC, English S, Yamada K, Yoo J, Murugesan R, Devasahayam N, Cook JA, Golman K, Ardenkjaer-Larsen JH, Subramanian S, Mitchell JB. Proc Natl Acad Sci USA 2002;99:2216. [PubMed: 11854518]

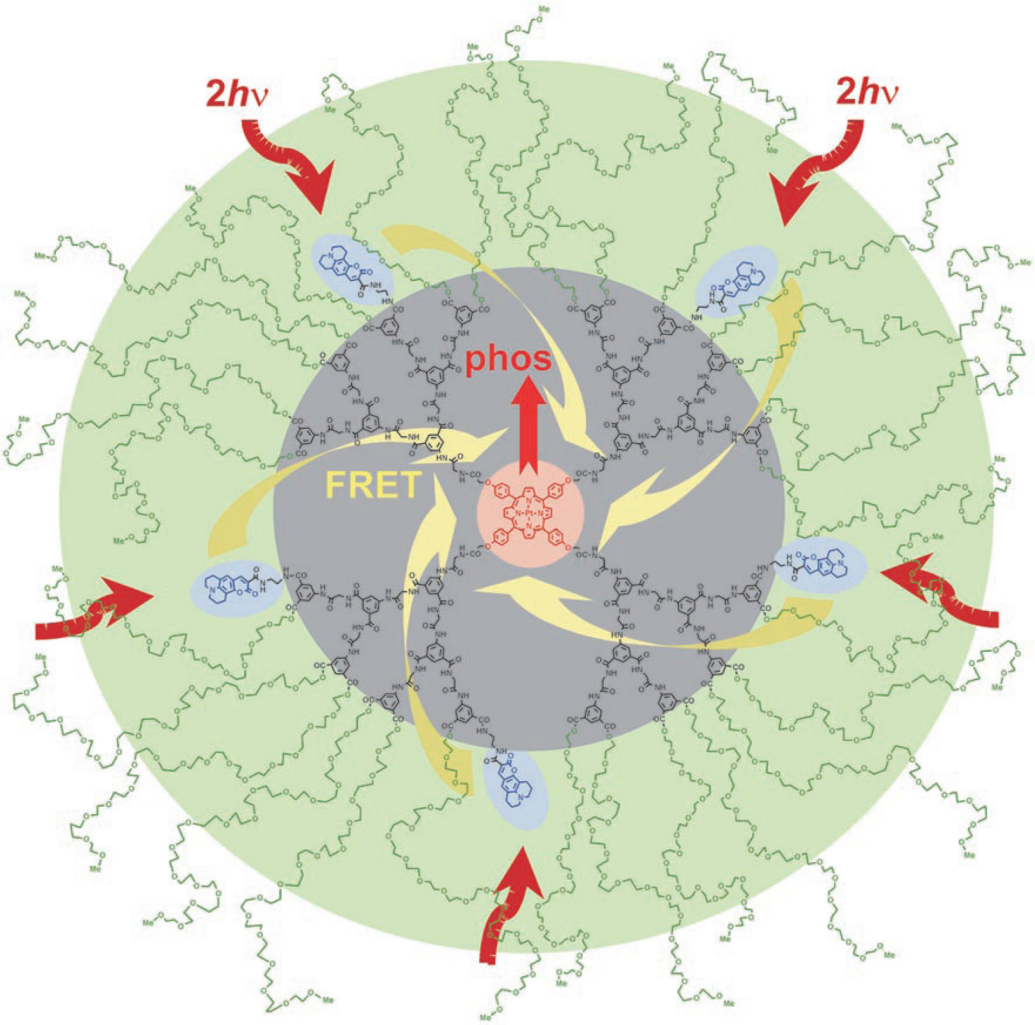

Figure 1.
Two-photon-enhanced oxygen probe PtP-C343 consisting of phosphorescent Pt *meso*-tetraarylporphyrin (PtP, red), several coumarin-343 units (C343, blue), polyarylglycine dendrimer (black) and peripheral oligoethylene-glycol residues (green). Arrows in the cartoon depict excitation of the C343 antenna *via* 2PA (brown), FRET (yellow) and phosphorescence of PtP-core (red).

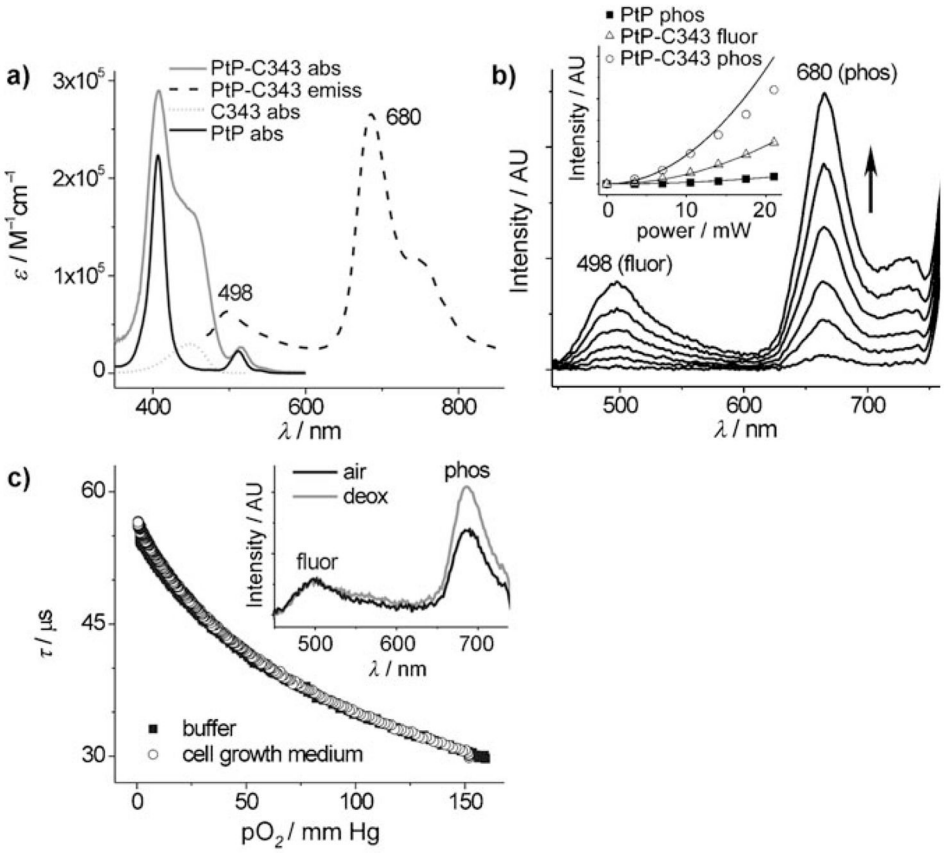

Figure 2.

Properties of nanoprobe PtP-C343. a) Absorption and emission (λ_{ex} = 460 nm, arbitrary intensity units) spectra of the probe and reference chromophores: PtP and C343. b) 2PA-induced emission spectra (excitation: λ_{ex} = 840 nm, 110 fs, 76 MHz rep. rate) at different excitation powers and power dependence (inset) for phosphorescence of a reference Pt porphyrin (PtP) without the antenna (black squares), PtP-C343 phosphorescence (white circles) and PtP-C343 fluorescence (white triangles). The data points [phosphorescence intensity (I), normalized by concentration, vs excitation power (P)], were fit to quadratic functions: $I(P) = aP^2$ (solid line). The phosphorescence deviates from the quadratic law at higher incident powers (see text and Figure 3). The fluorescence rises quadratically throughout the entire power range examined. c) Phosphorescence lifetime (τ) vs pO_2 calibration plots in pure buffer (black) and in cell growth medium containing 3 % of serum albumin (25 °C, pH 7.2) (white). Inset: 2PA-induced emission spectra (λ_{ex} = 840 nm) of the probe at air saturation (black) and in deoxygenated solution (gray), showing that only the phosphorescence signal (λ_{max} = 680 nm) responds to the change in oxygen pressure.

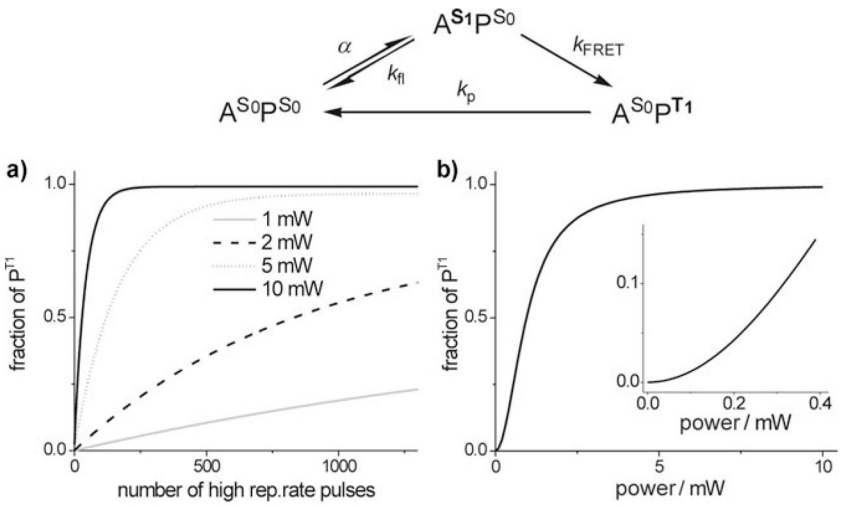

Figure 3.

Top: photophysical processes occurring in PtP-C343. a) calculated dependence of the fraction of excited triplet state molecules (P^{T1}) in the laser focal volume on the number of high repetition rate pulses (840 nm, 110 fs, 76 MHz) at different average laser powers; b) calculated dependence of P^{T1} in the focal volume on the average laser power under continuous train of high repetition rate pulses. The inset shows the region where the phosphorescence is proportional to the square of the excitation flux.

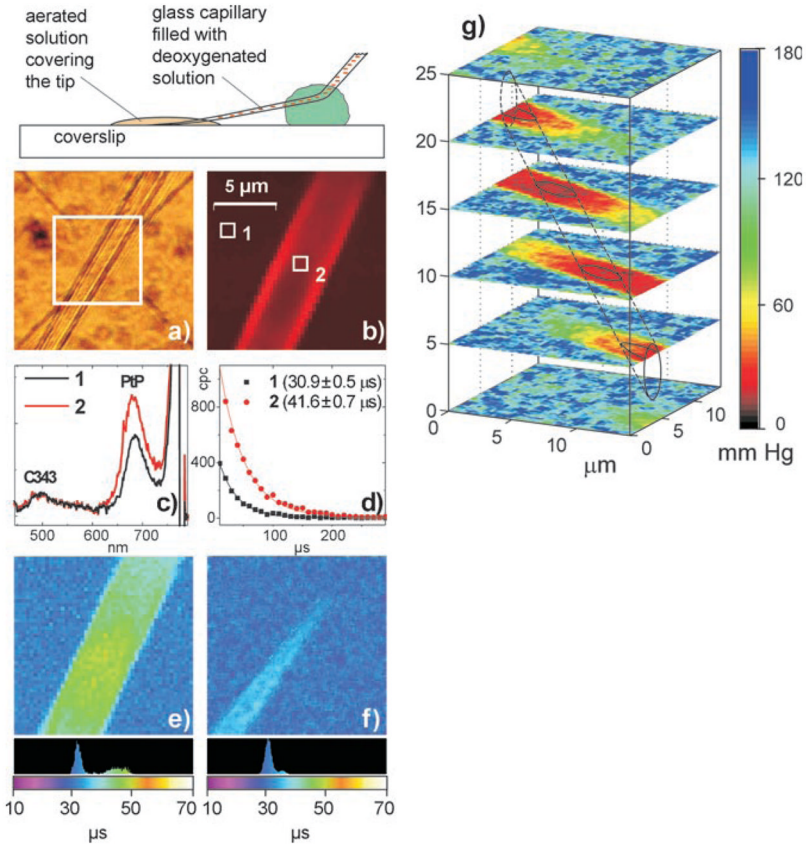

Figure 4.

Imaging of heterogeneously oxygenated objects. a) A section of the glass capillary, about 200 μm from the tip, as seen through the eyepiece of the microscope. b) Integrated phosphorescence intensity image (50 × 50 pixel^2) acquired under 2P excitation. c) Emission spectra from the areas **1** and **2** marked in image (b). d) Phosphorescence decays (CPC—counts-per-channel) in individual pixels in the regions **1** and **2** (1 μs gate, 100 gates per pixel, 50 ms pixel dwell time) and their fits to single-exponentials. Phosphorescence lifetime images of e) the capillary and f) the capillary tip. g) Stack of pO_2 images obtained by raster-scanning in ^{z}-axial planes (10 gates per pixel).

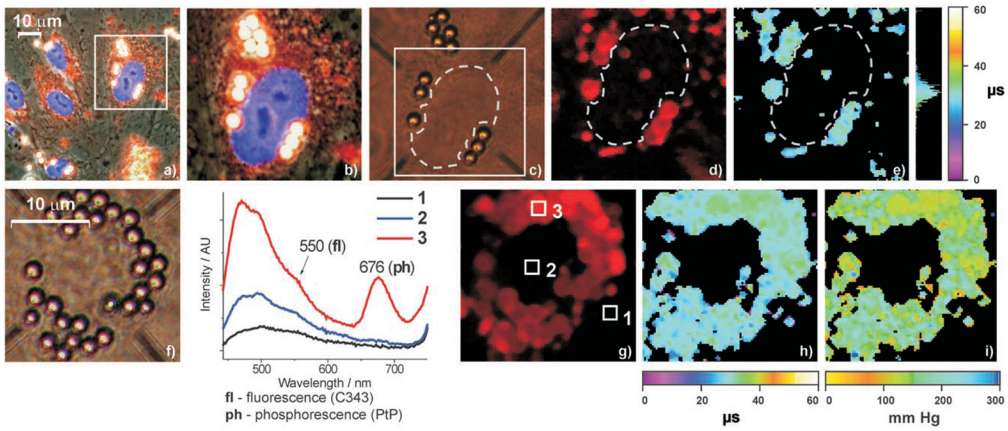

Figure 5.

Images of fixed (a–e) and live (f–i) human umbilical vein endothelial cells (EC) after induced co-internalization of 2 μm latex microspheres and PtP-C343. 87 ± 3 % of the total number of microspheres were internalized, of which 86 ±7 % contained PtP-C343. 2P excitation was the same as in the experiments (e, f) in Figure 4. a) Overlaid phase-contrasted and conventional fluorescence images show several cells with nuclei stained by a blue fluorescent dye (DAPI). The cell marked by the square contains several vesicles, where microspheres (white) are surrounded by the probe solution (red). b) Magnification (3.75-fold) of the perinuclear region of a selected cell. Small vesicles containing the probe, but no microspheres, appear as reddish dots around the nucleus. c) The same cell viewed through the eye-piece of the two-photon imaging microscope. The scanned area (square) and the nucleus (dashed line) are marked. d) Integrated intensity image of phosphorescence (50 × 50 pixels^2). e) Phosphorescence lifetime image. f) Nucleus of a cell surrounded by internalized micro-spheres. g) Integrated intensity image of phosphorescence and the emission spectra (to the left) collected from the areas 1–3 (marked by the squares). h) Phosphorescence lifetime image. i) pO_2 image calculated from the lifetime image (h).

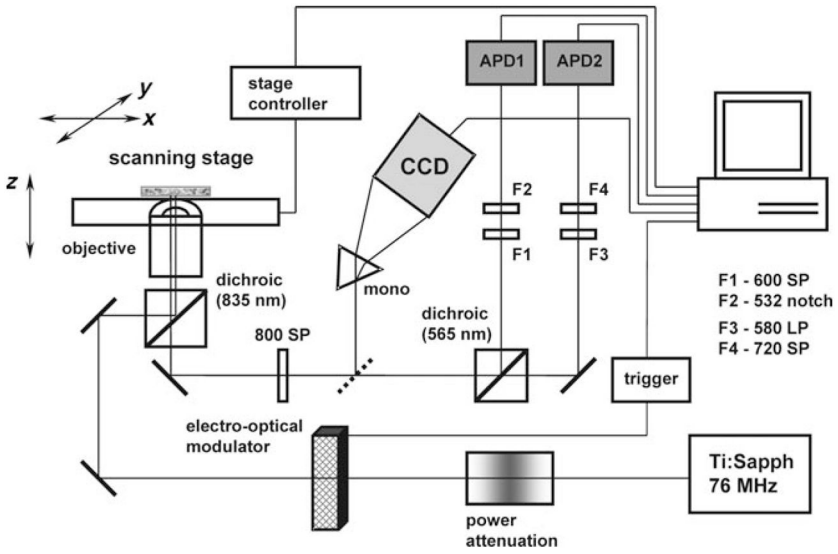

Figure 6.

Diagram of the imaging system. APD1 and APD2: avalanche photodiodes; F1–F4: short-pass (SP), long-pass (LP) and notch filters.